Biological and Medical Applications of Materials and Interfaces

Tightly Sealed 3D Lipid Structure Monolithically Generated on Transparent SU-8 Microwell Arrays for Biosensor Applications

Dong-Hyun Kang, Won Bae Han, Nakwon Choi, Yong-Jun Kim, and Tae Song Kim

ACS Appl. Mater. Interfaces, **Just Accepted Manuscript** • DOI: 10.1021/acsami.8b13458 • Publication Date (Web): 07 Nov 2018

Tightly Sealed 3D Lipid Structure Monolithically Generated on Transparent SU-8 Microwell Arrays for Biosensor Applications

Dong-Hyun Kang[†, ‡], *Won Bae Han*[†], *Nakwon Choi*[†], *Yong-Jun Kim*[‡], *and Tae Song Kim*[†, *]

[†]Center for BioMicrosystems, Korea Institute of Science and Technology, 5, Hwarang-ro 14-gil, Seongbuk-gu, Seoul, 02792, Republic of Korea

[‡]Department of mechanical engineering, Yonsei University, 50, Yonsei-ro, Seodaemun-gu, Seoul, 03722, Republic of Korea

KEYWORDS: artificial cell membrane, 3D lipid bilayer structure, freestanding lipid membrane, sealing, microwell arrays

Artificial lipid membranes are excellent candidates for a new biosensing platforms because their structures are similar to cell membranes and it is relatively easy to modify the composition of the membrane. The freestanding structure is preferable for this purpose since more manageable reconstitution of membrane protein. Therefore, most of the lipid membranes for biosensing are based on 2-dimensional structures that are fixed on a solid substrate (unlike floating liposomes) even though they have some disadvantages, such as low stability, small surface area, and potential retention of solvent in the membrane. In this paper, 3-dimensional freestanding lipid bilayer (3D FLB) arrays were fabricated uniformly on SU-8 microwells without any toxic solvent. The 3D FLBs have better stability and larger surface area due to their cell-like structure. In order to improve sealing characteristics of the 3D FLBs, the applied frequency of AC field was controlled during the electroformation. The 3D FLBs were observed through transparent SU-8 microwell arrays using confocal microscopy, resulting in perfect sealing until 5.5 days after the electroformation of more than 1 kHz. Also, the details of

the sealing of a fixed 3D freestanding lipid structure were discussed for the first time. Unilamellarity and biofunctionality of the 3D FLBs were verified by transport protein (α-hemolysin) assay.

1. Introduction

Lipids are a major component of all cell membranes, and they have key roles in most physiological processes, such as protecting cells, facilitating cell-to-cell communication, and contributing to metabolic activities[1-2]. These lipids are assembled into artificial membranes as spherical liposomes or 2-dimensional (2D) planar membranes in aqueous solutions in order to study, for example, protein-membrane interactions, membrane protein biosensing, and drug discovery because their structures are similar to real cell membranes, and they can be modified by reconstituting the proper membrane proteins for the desired applications[3-4].

One of the most fundamental research uses of lipid membranes as sensor platforms is planar lipid bilayers that are fixed on a solid substrate and have freestanding

structures, which makes it possible to study membrane-protein mediated transport across membranes, in particular, ion transport via ion-channels[5]. Despite the fact that planar freestanding black lipid membranes (BLMs) can be formed easily by various methods[5-7], their inherent fragility has prevented any further attempts to use them in robust detection systems. Therefore, the reduced size of the aperture in the planar-type devices that are used to increase the stability of membranes[5, 8] causes a severe reduction of the membrane area, which is the main disadvantage in attempts to conjugate a sufficient number of analytical elements to the membrane. In addition, since planar lipid bilayers are formed mostly by harmful organic solvents, the biomolecules, such as membrane proteins, might be damaged by the remaining solvent[9].

Another approach is then use of a liposome, especially giant unilamellar vesicles (GUVs) because they have relatively good stabilities, large surface areas, and large encapsulation volumes[3, 10]. Thus, they can conjugate and encapsulate large amounts of signaling molecules and membrane proteins, thereby amplifying the intensity of the signal. As a result, a one-to-one biological binding event is converted into a one-to-many signal, which greatly reduces the detection limits of the analytes[3]. However, even

though solvent-free GUVs can be made easily with various, simple, conventional methods, such as simple hydration[11-12] and electroformation[13-15], they have a wide range of size distributions (hydration: CV = 61.5%, electroformation: CV = 52.8%)[16]. Therefore, in sensor applications with GUVs, it is difficult to get reliable data due to the variations of the encapsulation volume and the surface area in each case. In addition, monitoring several GUVs simultaneously in the detection area of a microscope is rarely possible because they are floating in suspension, and they would have to land on the substrate randomly to be detected by microscopy. To overcome this weakness, some research has been reported in which GUV arrays were made on substrates[17-20]. However, most of the researchers used pre-fabricated GUVs or liposomes that they attached on the substrate by linking materials (i.e., polydiacetylene (PDA) and antibodies), which are relatively complicated and still have the issues of the variations of volume and surface area. For a narrow range of the size distribution of the GUV arrays on the substrate without linking materials, Kang[21] reported a simple method for fabricating arrays of controlled-size GUVs using patterned lipid by hydrogel stamp. However, attached GUVs on the substrate are not applicable in transport membrane

applications because the lipid tethers provide a pathway (via nanotubes, tens of nm) for the exchange of material, which creates a sealing problem between the inside and outside of the electroformed GUVs, hence only detached GUVs can be used for studies of the transport membrane. Osaki[22] reported a new trial of the monolithic fabrication of dome shaped or liposome-like structures that were attached directly to the shallow microwell substrate, but the dome shaped structure hardly keeps the interior solutions because leakage occurs from the attached region. Therefore, fully-closed liposome arrays were used as the form attached onto the substrate to prevent leakage, but they were easily detached and removed, which also creates problems for microscopic observation. As a result, even though sealing the 3D lipid structure that is attached to the substrate is important in membrane protein studies for sensor applications, to date, no one has reported sealing the 3D lipid structures fixed on the substrate. In our previous research, we reported that, for the first time, 3D GUV-shaped arrays with perfect sealing were grown monolithically on deep Si microwell arrays[23]. However, due to the opaque Si microwell, we were unable to study the details of lipid fusion or growth

behavior in the inner microwells, which were assumed to be closely related to the sealing characteristics using confocal microscopy.

In this study, we propose a new approach for generating uniform-sized, monolithic, 3-dimensional, freestanding lipid bilayers (3D FLBs) on a transparent SU-8 microwell array substrate without any organic solvent. Based on the transparent structure of the microwell, the sealing characteristics, which were a key issue for the assay of the protein membrane, were studied carefully by monitoring the inside of the microwell. In order to improve the sealing characteristics, it was found that the frequency of the AC field should be controlled during the electroformation stage. Consequently, a method for sealing is proposed for the first time that achieved sealings that lasted five days or longer in the 3D FLBs that were formed at a controlled frequency. In addition, the biofunctionality and unilamellarity of the generated 3D FLBs were verified by an assay in which we used a pore-forming protein.

2. Experimental section

2.1. Materials

All lipids were purchased from Avanti Polar Lipids, Inc. (Alabaster, AL, US), including 1,2-dioleoyl-sn-glycero-3-phosphocholine (DOPC) and 1,2-dioleoyl-sn-glycero-3-phosphoethanolamine-N-(lissamine rhodamine B sulfonyl) (Rhod-PE). The Alexa Fluor 488 dye (Succinimidyl Ester) was purchased from Thermo Fisher Scientific (Waltham, MA, US). The α-hemolysin from Staphylococcus aureus, sucrose, and all solvents were purchased from Sigma Aldrich (St. Louis, MO, US).

2.2. Fabrication of microwell array

We fabricated a microwell array on a silicon substrate using an epoxy-based photoresist. An epoxy-based photoresist (SU-8 3050, MicroChem Co., US) was spin coated on a 4-in silicon wafer at a thickness of 8 μm. After soft baking on a hotplate, the SU-8 was exposed to UV light using a mask aligner (Karl Suss MA6 Mask Aligner, Germany). The SU-8 was post-exposure baked (PEB) on a hot plate before developing.

The SU-8 was soaked in fresh SU-8 developer solution (SU-8 Developer, MicroChem Co., US) with agitation, and was rinsed with IPA.

2.3. Preparation of small phospholipid vesicle

A 1 ml portion of DOPC in chloroform (20 mM) containing a small fraction of Rhod-PE (0.5 mol%) for the observation of confocal microscopy was inserted into a glass vial. First, the chloroform was evaporated using N_2 blowing, and, then, the vial was placed under vacuum for at least 30 min. Then, the dry lipid film was hydrated with deionized (DI) water with gentle agitation. After the hydration of the lipid film, a suspension was obtained that contained multilamellar, micrometer-sized vesicles, and it was extruded 21 times through a 30 nm polycarbonate membrane filter (Nuclepore™ Track-Etched Membranes, Whatman®, UK) using an extruder (Avanti Polar Lipids, Inc., US). The SUV suspensions were stored at 4 °C for later use.

2.4. Selective deposition of lipids in the microwells

The technique of discontinuous dewetting was used to get lipid deposition only inside the microwell array[24-25]. A 30 μl droplet of the SUV suspension was caught between the microwell array and a glass blade. The glass blade had a small inclination angle (~15°) toward the dewetting line in order to maintain the droplet near the edge of the glass (Figure S1 in the Supporting Information). The glass blade was moved horizontally at a controlled speed. When the SUV suspension was dragged on the substrate patterned microwell array by the glass blade, the contact line was moving on the planar parts of the substrate without the deposition of SUVs, but it was pinned on the edges of the microwells due to the steep increase of the contact angle, which resulted in the trapping of SUVs in the microwells. After evaporation of the aqueous solution by a freeze dryer, the SUVs ruptured in the microwells, and then a multilayer film of the lipid was deposited selectively in the microwell arrays.

2.5. Electroformation in a simple microchannel

A simple, straight microchannel was designed for the hydration and electroformation of the selectively deposited lipid film. Also, a solution exchange for bioassay was accomplished easily by this microfluidic channel. The microfluidic channel was fabricated from polydimethylsiloxane (PDMS) using soft lithography techniques. PDMS can be used for the construction of microchannels because its transparency makes it suitable for optical detection, and it can be constructed easily into patterned channels via a molding process. To apply an AC electric field for electroformation, thin glass coated with indium tin oxide (ITO) was embedded into the PDMS microchannel. The height of the microchannel was 150 μm. The AC electric field was applied to the dried lipid film by a function generator (33210A, Keysight, US), and a 10 mM sucrose solution was added almost simultaneously to the dried lipid film by a syringe pump (NE-1000, New Era Pump Systems Inc., US). The sinusoidal AC electric fields were applied at various frequencies, ranging from 10 Hz to 100 kHz. The electric field that was applied was increased by 50 mV every 5 min until it reached 600 mV, after which the electric field was maintained more than 30 min at that level for the formation and sealing of the 3D FLBs. The flow rate was 20 μl/h during the electroformation. When the 3D FLBs

were fully grown on every microwell in the presence of an AC electric field that had various frequencies, a 10 mM solution of sucrose that contained 3 μM of Alexa Fluor 488 was injected along the microchannel in order to verify the sealing of the 3D FLBs.

2.6. Bioassay

In order to confirm the unilamellarity and biofunctionality of the membrane, an α-hemolysin assay was perfromed. The α-hemolysin monomers were dissolved in concentrations of 1, 3, and 5 μM in a 10 mM sucrose solution that contained 3 μM Alexa Fluor 488. After the sealing effect of the 3D FLBs was confirmed, the solution was exchanged with a solution that contained α-hemolysin. The passive transport of dye molecules across the pores formed by α-hemolysin heptamerization was monitored over time by confocal microscopy.

2.7. Imaging

To observe and analyze the 3D FLBs, we performed electroformation directly on the stage of the confocal microscope (LSM 700 confocal microscope equipped with ×40 c-apochromat (numerical aperture 1.2)) and fluorescence microscope (Zeiss LSM 5 PASCAL zxioplan 2 microscope equipped with appropriate filter sets ×10 epiplan-neofluar (numerical aperture 0.30), ×20 LD epiplan (numerical aperture 0.40), and ×50 LD epiplan (numerical aperture 0.50) objectives (ZEISS)). The images were captured using a Retiga6000 CCD camera from Qimaging (Surrey, BC, Canada) and Qimaging pro software (version 7.0). Scanning electron microscopy (SEM, NOVA) measurements were performed on the SU-8 patterned Si substrates in order to obtain the dimensions of the microwells.

3. Results and discussion

3.1. 3D FLB formation

In our previous research, the 3D lipid structure was generated successfully in the array of silicon microwells[23]. However, in this study, as shown in Figure 1a, a micro-

device with arrays of microwell structures was fabricated by using a transparent polymer (SU-8) on a silicon substrate, and confocal microscopy was used to monitor the change in the lipid structure deep inside the microwell during each sequence of the formation of the 3D FLBs, which is the key point of sealing the 3D FLBs. In order to produce arrays of 3D FLBs, small unilamellar vesicles (SUVs) in aqueous solution were filled selectively only inside the microwell and dried for the deposition of lipid multilayer films in the microwell arrays (Figure 1b). Using this technique, we were able to pattern the stacked lipid film in the microwells without any toxic solvent. As shown in a fluorescence microscope image and their intensity scanning graph of Figure 1c and d, the amounts of the selectively-deposited lipid were very uniform over a large area (~cm^2) for the fabrication of the 3D FLBs arrays with high density (~300,000 cm^{-2}).

Figure 2a shows a schematic illustration of the sequence during the generation of the 3D FLBs. As discussed in our previous research, the stacked lipid film initially started to self-spread (Figure 2a, i and ii) upon rehydration under exposing to an AC electric field during the electroformation process[23]. After the self-spreading of the lipid bilayer, several multilamellar vesicles (MLVs) were generated on each microwell, and they were

tethered to the bottom of the substrate (Figure 2a, iii). The growth of these vesicles was time dependent, and they became close to each other due to the confined space of the microwell (Figure 2a, iv). Then, these vesicles underwent gradual fusion with neighboring vesicles (Figure 2a, v and vi). The fusion of the vesicles was monitored during each sequence by confocal microscopy due to the transparent microwells, as shown in Figure 2a. Eventually, the 3D FLBs were formed on each microwell. The shape of the 3D FLBs that were generated on microwells was a semispherical structure that was fixed on the entrance of each microwell, as shown in Figure 2b. In terms of sealing characteristics of the generated 3D FLBs on microwells, it is very important to fix the 3D FLBs tightly in the microwells. The details of the sealing characteristics are described in following sections 2.2 and 2.3.

To evaluate the 3D FLBs on the microwell arrays, we measured the numbers and sizes of the structures that were generated at the various frequencies. The size of a 3D FLB was defined as the diameter of a fixed semispherical structure (Figure 2c), and it was measured by confocal microscopy after electroformation. The histograms in Figure 2c show these size distributions at various frequencies, ranging from 10 Hz to 100 kHz.

Each dataset was fitted with the Gaussian distribution function to obtain the standard deviation of the average diameter. In the case of electroformed GUVs on planar substrates, the sizes of the vesicles decreased, and the distribution became narrowed as the AC frequency was increased until the optimum frequency for electroformation was reached[26]. However, in this study, when the frequency range was 10 Hz to 1 kHz, the mean diameters of the 3D FLBs were similar (about 15 μm) irrespective of the frequency. We concluded that the lipid structure was determined by the wall of the microwells because the 3D FLBs were formed in microwells that had limited volume, which resulted in their having a uniform size. At higher frequencies (10 to 100 kHz), the mean diameter of the 3D FLBs was smaller, and the widths of the Gaussian fits were widened because of the exceeding of the optimum frequency for electroformation, and there was a good match with the case of the electroformation of GUVs on planar substrates[27]. At 10 and 100 kHz, the measured mean diameters of the 3D FLBs were 11.73 ± 1.84 μm (mean ± S. D.) and 11.32 ± 2.25 μm (mean ± S. D.), respectively. In conclusion, the frequency range of 10 Hz to 1 kHz led to the formation of 3D FLBs with the narrowest size distribution (15.89 ± 2.25 μm, CV: 13.85% at 1 kHz). These results

indicated the importance of the structure of the microwell and variations in the AC frequency for the formation of the monodispersed array of 3D FLBs.

3.2. Sealing and AC filed effect

Since the 3D FLB array seems to be a powerful platform for the assay of ligand-binding of membrane protein incorporated in lipid membranes, it is very important to study their sealing characteristics. In order to determine the sealing of the generated 3D FLBs, fluorescent dye (Alexa Fluor 488) was infused through the microchannel after completion of the electroformation process and monitored over time by confocal microscopy, as shown in Figure 3a. After the fluorescence dye arrival in the 3D FLBs, at 10 Hz and 100 Hz, they moved into the 3D FLBs through the unwanted crack even though the start times were different (more details in 0 s to 300 s at 10 Hz and 900 s to 1200 s at 100 Hz were shown in Figure S2 in the Supporting Information). However, at 1 to 100 kHz, the fluorescent dyes did not enter into the 3D FLBs, and the sealing of the 3D FLBs was maintained. The time-dependent changes in the normalized intensities of the inside of the 3D FLBs with various frequencies are shown in Figure 3b. The

normalized intensity of the 3D FLBs formed during 10 Hz condition increased very sharply after the Alexa Fluor 488 reached to the 3D FLBs because the fluorescent dyes moved into the 3D FLBs without any time intervals. For the case of the 3D FLBs that were formed at 100 Hz, the 3D FLBs seemed to be sealed when the Alexa Fluor 488 arrived, but their sealing was not maintained as time passed, which is the major case of sealing to leaky transition at 100 Hz. Some minor cases of sealing to leaky transition also were observed, and they are explained in detail in the Supplementary Information (Figure S3 in the Supporting Information). Conversely, above 1 kHz, the normalized intensities did not increase as time passed, and the slight increase of the normalized intensity at 1 to 100 kHz was background noise associated with the introduction of the fluorescent dye. Perfect sealing was achieved above 1 kHz of electroformation, indicating that the AC frequency during the electroformation process is the key factor in sealing the 3D FLBs.

As mentioned earlier, since the 3D FLBs were fixed on the mirocwell, unwanted leakage possibly could occur at the cylindrical lipid structure, which is region where the 3D FLBs are attached on the substrate. In order to identify the relationship between the

sealing and attaching regions of the 3D FLBs on the substrate, side view images of the 3D FLBs reconstructed by scanned confocal microscopy images were observed as AC frequency (Figure 4a). At more than 1 kHz (the sealing case), the semispherical lipid structure located outside of the microwell became spherical, and the cylindrical lipid structure located inside of the microwell expanded and contacted the surface of the microwell. However, at 10 and 100 Hz (the leaky case), the semispherical lipid structure became prolate or oblate, and the cylindrical lipid structure became lipid tether or thin cylindrical structures so that it did not contact the surface of the microwell.

To clarify the change in the morphology of the 3D FLBs on the microwell arrays as AC frequency, the vesicle deformation theory in the AC field[28-29] was used in our case, and then, we verified the suitability of this theory in the sealing of the 3D FLBs on SU-8 microwell arrays. We assumed that the change in the morphology of the semispherical lipid structure (outside the microwell) promoted changes of the cylindrical lipid structure (inside the microwell). Figure 4b shows a schematic representation of the single 3D FLBs and the definitions of the pole and the equator. When an AC electric field was generated on the 3D FLBs, the lipid membranes received forces that were acting in

different directions at various frequencies, because the lipid membranes are electrical insulators and act as capacitors[30]. The response of the membranes to the electric fields related to the dynamic physical processes that were occurring on a different time scale[28, 30]. A vesicle polarizes on the Maxwell-Wagner time scale, t_{MW}, which can be written as follows:

$$t_{\mathrm{MW}} = \frac{\varepsilon_{\mathrm{in}} + 2\varepsilon_{\mathrm{ex}}}{\lambda_{\mathrm{in}} + 2\lambda_{\mathrm{ex}}} \quad (1)$$

where ε_{in} and ε_{ex} are the dielectric constants, and λ_{in} and λ_{ex} are the conductivities of the solutions inside and outside of the 3D FLBs, respectively. The lipid bilayer is impermeable to ions, so free charges accumulate on both sides of the membrane. Therefore, the vesicle acts as a capacitor, and it charges on a time scale, t_c, that can be written as follows:

$$t_{\mathrm{c}} = RC_{\mathrm{m}}\left(\frac{1}{\lambda_{\mathrm{in}}} + \frac{1}{2\lambda_{\mathrm{ex}}}\right) \quad (2)$$

where R is the radius of the 3D FLB and C_m is the capacitance of the membrane. The time required to charge the capacitor, t_c, typically is much longer than the Maxwell-Wagner time, t_{MW}. These time scales are very important for understanding the dynamic response of 3D FLBs that are subjected to the frequency-dependent morphology

changes of the lipid structure. Since frequency is defined as the inverse of the time scales in Equations (1) and (2), we defined the Maxwell-Wagner frequency, ω_{MW}, and the capacitor charging frequency, ω_c. In this study, 3D FLBs were formed in a 10 mM sucrose solution. Therefore, the conductivities and dielectric constants of the inside and outside of the 3D FLBs had the same values (λ_{in} and λ_{ex} = 0.01 mS/m, and ε_{in} and ε_{ex} = 80). For the calculation of ω_{MW} and ω_c, R and C_m were fixed as 7.5 μm and 1 μF/cm^2, respectively [30-31]. The calculated values of ω_{MW} and ω_c were 2247.95 Hz and 14.15 Hz, respectively.

At low frequencies, $\omega < \omega_c$ and the large membrane impedance obstructs the current that is flowing into the interior of the 3D FLBs, and the electric fields are distributed to avoid the membrane, as shown in Figure 4c, i). Due to the geometry of the 3D FLBs, the semispherical lipid structure is squeezed at the equator and pulled at the poles by the radial Maxwell stress, τ_{MW}, or the pressure, p_{MW}, that arises from the tangential electric field, hence the structure of the semispherical lipid becomes a prolate shape. In the intermediate frequency regime, i.e., $\omega_c < \omega < \omega_{MW}$, the displacement currents flow across the membrane, which is capacitively short-circuited. Therefore, the electric field

lines penetrate the interiors of the 3D FLBs, and the interactions of the tangential and normal electric fields with the free charges produce tangential and normal forces, i.e., f_θ and f_r, respectively. As mentioned above, the conductivities of the inside and outside of the 3D FLBs are the same in the ideal condition. However, in actual systems, the internal and external conductivities are different in the specific local area. Therefore, the charge densities on the inside and outside membrane interfaces become imbalanced. Depending on the charge densities of the 3D FLBs, f_θ is directed toward the poles or the equator, and f_r is directed towards or away from the electrodes, leading to prolate shapes ($\lambda_{in} > \lambda_{ex}$, Figure 4c, ii)) or oblate shapes ($\lambda_{in} < \lambda_{ex}$, Figure 4c, iii))[28-29]. At high frequencies, $\omega > \omega_{MW}$, the charge density of the lipid membrane has small values because the electric charges cannot follow the oscillations of the electric fields. As a result, the net charge density of the lipid membrane decreases as the field frequency increases, hence the semispherical lipid structure becomes spherical in shape, as shown in Figure 4c, iv).

Since the 3D FLBs are fixed on the microwells in contrast with floating vesicles, the morphology changes of the semispherical lipid structures cause changes of the

cylindrical lipid structure that is the bottom side of the 3D FLBs in the microwells. To minimize their membrane tension and stress (energy minimization approach in the lipid membrane)[32], the cylindrical lipid structures are transformed as lipid tether structures or thin cylindrical structures that provide a pathway for exchanging the materials between inside and outside of the 3D FLBs in the prolate case, and they are expanded in oblate and spherical cases, as shown in Figure 4a and c. At more than 1 kHz (sealing case), the cylindrical lipid structure expanded and contacted the self-spreading lipid bilayer on the SU-8 microwell surface (where the lipid bilayer self-spreads on the substrate in the initial hydration stage).

In order to check the suitability of the vesicle deformation theory in an AC field to the 3D FLBs and confirm the frequency variation, we defined the shape change as an a/b ratio, where a and b are the vertical and horizontal radii of the semispherical lipid structure, respectively (Figure 4c). The experimental data of Figure 4d indicate the values at which the shape of the 3D FLBs changes as the frequency increases. The calculated values of ω_c and ω_{MW} were 14.15 Hz and 2247.95 Hz, respectively. By contrast, the experimental values of ω_c and ω_{MW} were approximately 15 Hz and 1 kHz,

respectively. When the applied AC frequency was lower than 15 Hz ($\omega < \omega_c$), the shape of the 3D FLBs was prolated. At the intermediate frequency ($\omega_c < \omega < \omega_{MW}$), the coexistence of prolated and oblated shapes was observed. When the applied AC frequency was higher than 1000 Hz ($\omega > \omega_{MW}$), the shape of the 3D FLBs became spherical. Even though the theoretical and experimental values of ω_{MW} were a little different, the change in the shape of the 3D FLBs showed that the vesicle deformation theory in AC fields was able to match the 3D FLBs. Also, the shape change of the 3D FLBs had the same tendency as the vesicles floating in free space in the AC fields[28-29], although the absolute value became relatively lower due to the structural difference, and we observed that this shape change caused the change in the structure of the cylindrical lipid, which was the key to determining the sealing characteristics of the 3D FLBs.

3.3. Sealing method by membrane fusion

It is apparent from the results described above that the sealing of the 3D FLBs was observed when the cylindrical lipid structure expanded and contacted the self-spreading

lipid bilayer at more than 1 kHz (high frequency). However, the 3D FLBs were not sealed with a simple contact between the cylindrical lipid structure and the self-spreading lipid bilayer. This decision was made because a water layer naturally exists between the lipid membranes, and it provides a pathway for material exchange[33] from the outside of the 3D FLBs to the unwanted leakage at bottom of the cylindrical lipid structure, where the 3D FLBs are attached to the substrate. In addition, the water layer between the lipid membranes disturbs membrane fusion[34]. Therefore, we assumed that the close contact between the self-spreading lipid bilayer and the cylindrical lipid structure (Figure 4a) caused by the changes in the morphology of the 3D FLBs at the high frequency of electroformation promoted membrane fusion, which is the main point of the tight sealing of the 3D FLBs. Figure 5a shows the close contact and fusion of the membrane caused by the changes in the morphology of the 3D FLBs, which is the basis of our hypothesis for the sealing of the 3D FLBs. Due to the changes in the morphology of the 3D FLBs in an AC field, the cylindrical lipid structure expands and approaches the self-spreading lipid bilayer. These changes promote close contact between the lipid bilayers, thereby reducing the water layer (leaky gap) between membranes. When the

close contact occurred in the presence of the AC field, the polar heads of the lipids in the outer leaflets fuse to form a stalk-like structure, which extended to create a diaphragm[34]. The forces generated by the extension of the diaphragm promoted the fusion of the inner leaflets and the creation of a fusion pore[34]. After the membrane fusion was partially initiated, the fused area was widened by the tension on the membrane that was generated by the close contact between the lipid bilayers. Then, the cylindrical lipid structures of the 3D FLBs and the self-spreading layer were fused completely. The sealing of the 3D FLBs was achieved after the complete fusion because there is no longer a water layer (leaky gap) to provide a pathway that would allow the molecules to move.

In order to verify these sealing characteristics, which are closely related to the fusion of the membrane between the 3D FLBs and the self-spreading layer, we used a method published by Akashi[35]. This method involves the fluorometric estimation of lamellarity, which is based on the quantification of the intensity of the incorporated fluorescently-labeled lipids in the membranes. The intensities of the fluorescence of the cylindrical lipid structure located in the inner microwell were measured by confocal microscopy to

detect their lamellarity. In addition, to clarify the relationship between lamellarity and the intensity of the fluorescence of the lipid membrane (0.5 mol% Rhodamin tagged), we also measured several cases of the intensity of the 3D FLBs for comparison. When the 3D FLBs were not fully grown by electroformation, they were composed of multilayer lipid membranes. The fluorescence intensity was 209 at the multilayer (lamellarity: 3+) (Figure S4a in the Supporting Information) and 137 at the two lipid membrane (lamellarity: 2) (Figure S4b in the Supporting Information). However, when the 3D FLBs were fully grown and fused, they were composed of unilamellar lipid membranes (lamellarity: 1), which was verified by the α-hemolysin experiment in Section 3.4., and their fluorescence intensity was 87 (Figure S4b and c in the Supporting Information). Based on these results which provided the correlation between fluorescence intensity and lamellarity, we were able to confirm that the complete fusion of the cylindrical lipid structure and the self-spreading lipid bilayer had occurred. After the electroformation process at the frequency of 1 kHz, fluorescent dye (Alexa 488) was infused through the microchannel to check the sealing of the 3D FLBs, and the intensity of the cylindrical lipid structure was measured for each sealed and leaky case, as shown in Figure S5. In

the sealed case, the fluorescence intensities of the semispherical lipid structure and the cylindrical lipid structure were almost the same. However, in the leaky case, the fluorescence intensity of the cylindrical lipid structure was higher than that of the semispherical lipid structure. To identify the lamellarity of the lipid structures located inside the microwell, the highest values of fluorescence intensity were measured for 50 sealed cases and 50 leaky cases by scanned confocal microscopy images, as shown in Figure 5b. For the sealed case, the intensity of the lipid membrane located inside the microwell was 80.74 ± 11.94. However, the intensity of the leaky case was 144.60 ± 24.26, which was higher than that of the sealed case by a factor of about 1.8. Based on the correlation between the intensity of the fluorescence and the lamellarity, the lamellarity of the lipid membranes located inside the microwell was estimated to be 1 for the sealed case and 2 for the leaky case. The fact that the cylindrical lipid structure was not fused completely in the leaky case means that the lipid membranes of the leaky case did not have unilamellar lipid structures (i.e., multilayer structures), which indicated the existence of an unexpected leaky gap (a water layer that measured in the tens of nanometers) between the multilamellar lipid membranes. However, in the sealed case,

the cylindrical lipid membrane was fused completely with the self-spreading lipid bilayer, and it formed a unilamellar membrane. The completely fused membrane sealed the 3D FLBs due to the absence of the water layer between the lipid membranes for material exchange, which proved our hypothesis for the sealing of the 3D FLBs.

In order to verify the stability of the sealing, fluorescence dye (Alexa Fluor 488) was encapsulated in the 3D FLBs during the generation step. After the generation step, a solution was exchanged as a 10 mM sucrose solution and the stability of the sealing was observed by fluorescence microscopy. The 3D FLBs maintained their sealing for 133 h (about 5.5 days) even under the flow conditions in the microfluidic channel. In addition, the stability of the sealing was maintained during several solution exchanges. This was attributed to their closed shape without any bilayer edges that were exposed directly to the aqueous solution and to their flexible 3D shape that was able to release external pressure and membrane tension. Based on these results, we concluded that the 3D FLBs, due to their 3D structures, were more stable than 2D BLMs, indicating that the 3D FLBs can be used in future attempts to develop robust detection systems.

3.4. Transport protein assay

In order to verify the possibility of analyzing membrane transport with the aid of a transport protein, we used α-hemolysin, a toxic membrane protein that binds to the lipid bilayer and forms transmembrane nanopores. The diameters of the transmembrane nanopores that are formed by α-hemolysin are in the range of 1-2 nm[36]. The transport activity of α-hemolysin often is used to confirm the formation of a thin lipid bilayer (4-5 nm), because α-hemolysin acts as a transport protein only when the nanopores penetrate the bilayer lipid membrane[37]. After generating 3D FLBs at 1 kHz and confirming the sealing and the unilamellar structure, the solution containing dissolved α-hemolysin was infused through the microchannel. We used α-hemolysin at three different concentrations, i.e., 1, 3, and 5 μM. The α-hemolysin monomers were dissolved in a 10 mM sucrose solution that included 3 μM Alexa Fluor 488. While the α-hemolysin monomers are soluble in solution, once bound onto a lipid bilayer, α-hemolysin assembles into a heptameric ring and forms a nanopore[36]. The Alexa Fluor 488 diffuses into the 3D FLBs through this nanopore when the α-hemolysin is bound

onto a lipid bilayer. We used confocal microscopy to monitor the intensity of the fluorescence of the Alexa Fluor 488 on the inside of the 3D FLBs. Figure 6a shows the normalized intensity of the Alexa Fluor 488 diffused in the 3D FLBs by the α-hemolysin nanopores. Without the α-hemolysin, the normalized intensity does not increase. However, when the α-hemolysin reached the lipid bilayer and formed nanopores into it, the inside intensity of the 3D FLBs increased because of the diffusion of the fluorescence dye molecules through the α-hemolysin nanopores. At a high concentration, the α-hemolysin monomers quickly formed heptameric nanopores in the lipid bilayer because of their frequent exposure to the membrane. Therefore, at a 5 μM concentration of α-hemolysin, the α-hemolysin nanopores were formed in a relatively short time (~ 600 s), and then the normalized intensity increased very sharply because many α-hemolysin nanopores were opening, and the Alexa Fluor 488 diffused vigorously into these nanopores. However, when the concentration of α-hemolysin was 1 μM, the α-hemolysin nanopores were formed relatively slowly because of their low concentration. The normalized intensity started to increase after 2000 s, and then it increased gradually at 1 μM. Figure 6b shows the confocal microscopy images of the

3D FLBs after the 1 μM concentration of α-hemolysin was reached. The insides of the 3D FLBs were filled gradually by Alexa Fluor 488 through the α-hemolysin nanopores. These results indicated that the generated 3D FLBs were unilamellar, and our micro-device can be used for the analysis of membrane transport with the aid of a transport protein.

4. Conclusion

In this paper, we presented a novel method for generating 3D FLBs as a uniform-sized array (diameter: 15.89 μm, CV: 13.85% at 1 kHz) on transparent polymer microwell arrays without any solvent by using rehydration and electroformation of a selectively deposited lipid film in each deep microwell with high density (~300,000 cm^{-2}). Since the generated 3D FLBs were fixed on the microwells, the cylindrical lipid structure, which was located inside of the microwells, was essential for achieving perfect sealing. For firmly attached cylindrical lipid structure to the surface of the microwell, the morphology of the 3D FLBs was changed by various AC frequencies, and

our numerical calculations strongly supported the experimental results. Based on our monitoring using confocal microscopy, the 3D FLBs were deformed as prolate shapes at low frequency (10 Hz), prolate and oblate shapes co-existed at the intermediate frequency (100 Hz), and the spherical shape existed at high frequencies (1 – 100 kHz). When the 3D FLBs was deformed as in the prolate shape, the cylindrical lipid structure was contracted and became a thin and tethered structure, which caused the unsealing of the 3D FLBs. However, the cylindrical lipid structure was expanded and contacted the self-spreading lipid bilayer in the oblate and spherical cases, and, then, the 3D FLBs were sealed tightly by the fusion between the cylindrical lipid structure and the self-spreading lipid bilayer. This was confirmed by measurements of the fluorescence intensity by scanning all of the cylindrical lipid structures in the microwells to check for lamellarity. The 3D FLBs maintained their sealing for 5.5 days, even under a flow condition in the microfluidic channel, which indicated their improved stability when compared with 2D free standing BLM devices. Unilamellarity and biofunctionality were verified by assaying the transport protein (α-hemolysin). Thus, a method for sealing of 3D lipid structures grown in deep microwells is proposed for the first time in this study.

Since the generated 3D FLBs had a more stable structure and a larger surface area than the 2D freestanding BLM devices, they are able to use a very powerful platform to biosensor applications using membrane proteins. For example, reconstitution of ion channels with the 3D FLBs will be a good candidate for biomimetic tongue or nose applications. Also, because it is relatively easy to modify the composition of the membrane, the proposed 3D FLB array platforms are good candidates for model membrane experiments that verify functions of proteins and neurotransmitters in studies of brain functions.

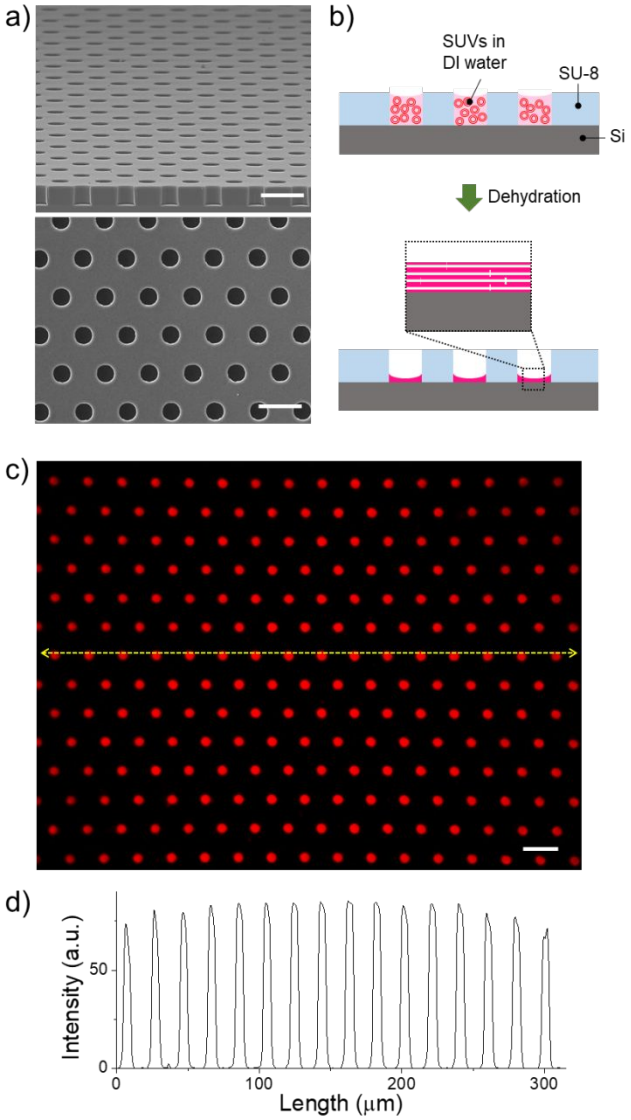

Figure 1. Selective deposition of the lipid multilayer only inside microwells. a) SEM images of fabricated SU-8 microwell arrays on a silicon substrate. The diameter and the depth of the microwell were 8 μm, and the pitch of each microwell was 20 μm. b) Schematics of selective deposition on the microwells. After filling the SUVs only inside of microwells, the chip was placed in the freeze dryer for dehydration. After the

dehydration, the stacked lipid film was deposited selectively only inside of microwells. c) Fluorescence microscopy image of selectively deposited lipid after the dehydration. d) Fluorescence intensity profile along the dotted line in c). All scale bars are 20 μm.

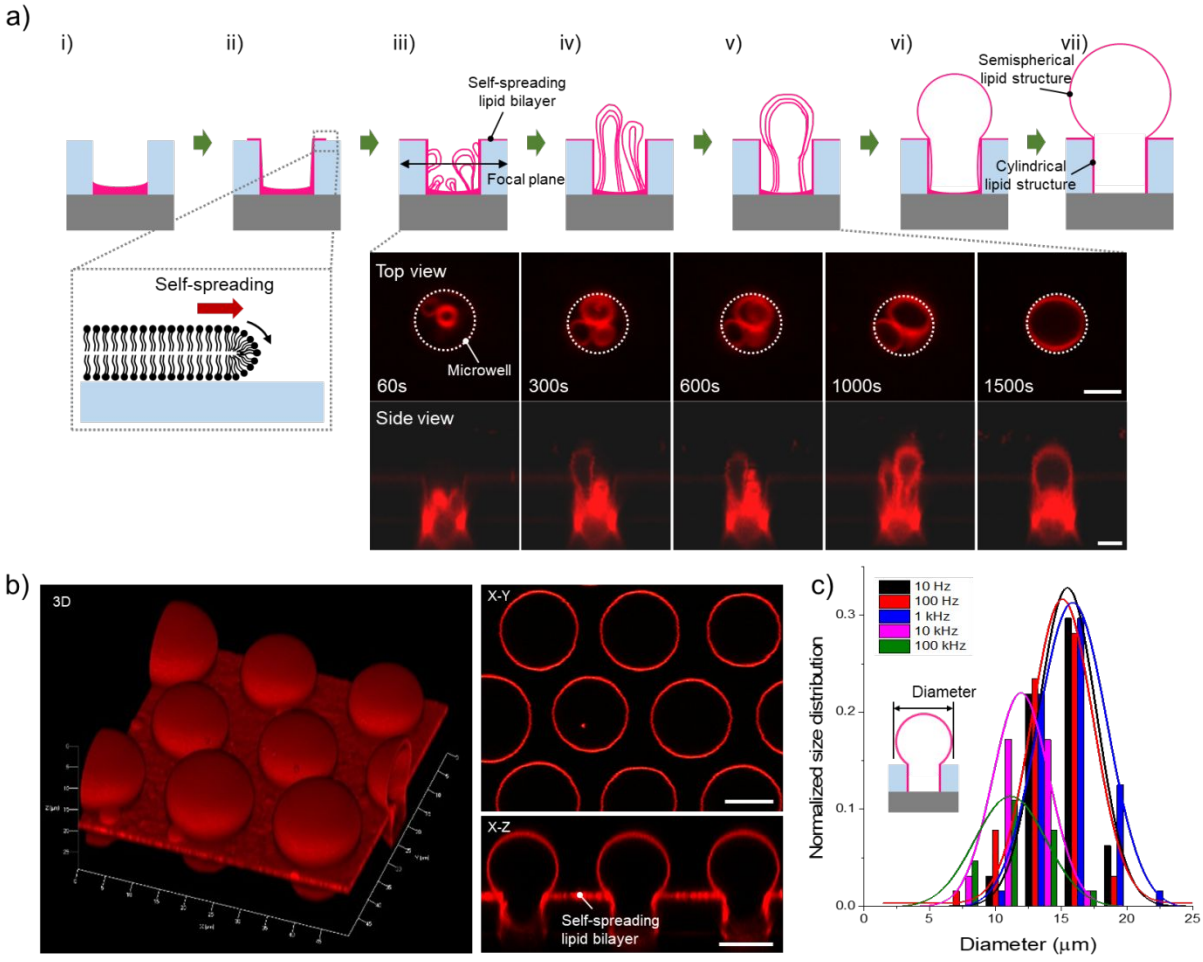

Figure 2. The generation of 3D FLBs by rehydration and electroformation. a) Schematics of the generation of 3D FLBs: i) The deposited lipid multilayer. ii) At the

beginning of rehydration and electroformation by 10 mM sucrose solution, the stacked lipid film was self-spread initially. iii) After the self-spreading of the lipid bilayer (covering the entire surface of the SU-8), the lipid film was swelling and several MLVs were generated that were tethered to the substrate. iv) The MLVs were grown and fused by several multilayer structures. v) As time passed, the growing multilayer structures got closer to each other due to the confined space of the microwell, and they fused to become one multilayer structure. vi) Then, the multilayer structure underwent gradual fusion and formed a unilamellar structure. vii) Finally, the 3D FLBs were formed on the microwell. The lower images were obtained by confocal microscopy at 1kHz. The focal plane was inside the microwell, hence we were able to monitor each sequence of the generation and fusion of the 3D FLBs. The scale bar is 5 μm. b) The confocal microscopy images of generated 3D FLBs as 1kHz electroformation frequency. The 3D image was reconstructed from scanned confocal microscopy images. Thin and identical fluorescence intensities of the structures in X-Z imply that each of the 3D FLBs consisted of a single bilayer. The scale bar is 10 μm. c) The size distributions of the 3D

FLBs at various frequencies (10 Hz – 100 kHz). Each dataset was fitted with the Gaussian distribution function.

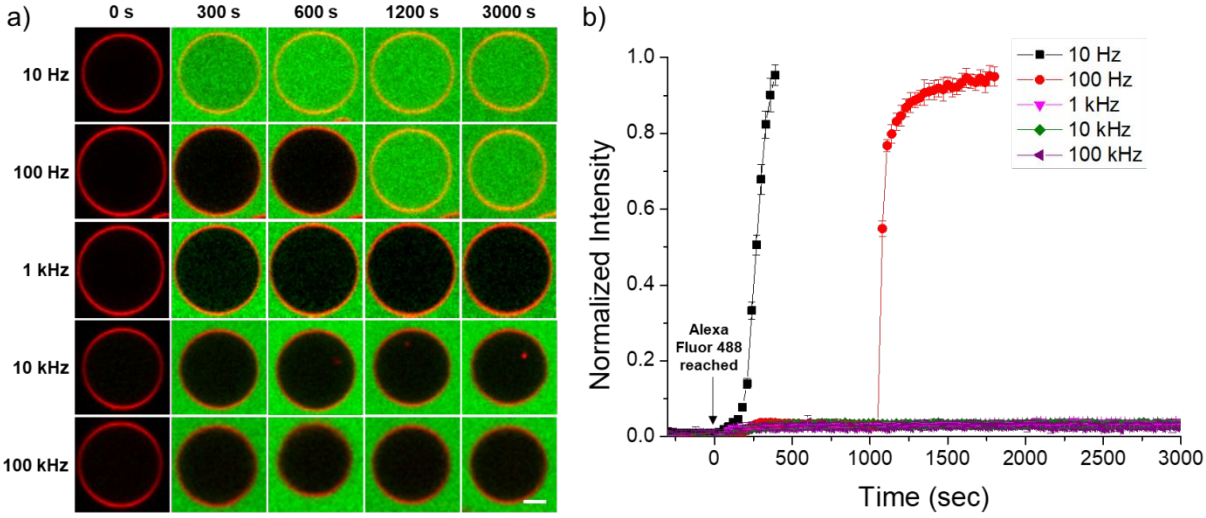

Figure 3. The sealing characteristics of the 3D FLBs at various frequencies. a) Images of the 3D FLBs observed by confocal microscopy over time at various electroformation frequencies. At 0 s, the Alexa Fluor 488 was reached. The scale bar is 5 μm. b) The normalized intensity of the inner 3D FLBs after the Alexa Fluor 488 was reached. The error bar represents the standard deviation (n ≥ 4). At 10 and 100 Hz, external fluorescent dye molecules entered inside the 3D FLBs and increased the normalized intensities because of their leaky structures. Above 1 kHz, the sealing was maintained.

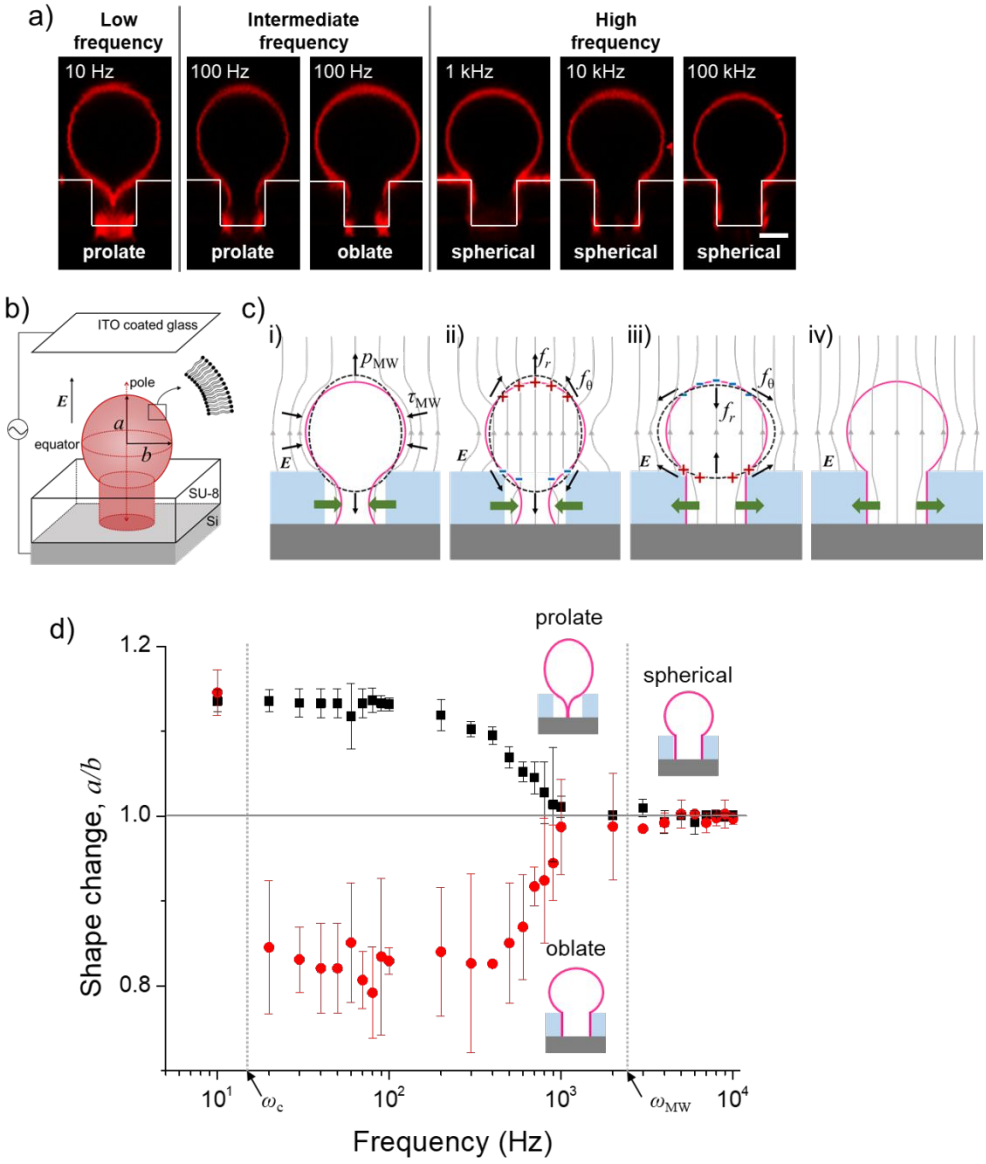

Figure 4. The shape of 3D FLBs at the various electroformation frequencies. a) Side view of the generated 3D FLBs observed by confocal microscopy as frequencies. The side view images were reconstructed from the scanned confocal microscopy images. Tethered and thin cylindrical lipid structures were observed at 10 Hz and at the prolate

case of 100 Hz, respectively. At the oblate case of 100 Hz and the spherical case of 1 to 100 kHz, the cylindrical lipid structure was expanded and contacted the self-spreading lipid bilayer. The scale bar is 5 μm. b) The geometry of the 3D FLB, and c) the net charge distribution at the 3D FLB interfaces. At low frequencies, the 3D FLBs were squeezed by the radial Maxwell stress or pressure arising from the tangential electric field, hence the 3D FLBs adopt a prolate shape i). At intermediate frequencies, due to the difference in the conductivity conditions, the net charges across the membrane, illustrated with pluses and minuses, differed depending on the values of the conductivity inside and outside of the membrane. The forces applied to the charges by the normal and the tangential electric fields deformed the 3D FLBs into prolates for $\lambda_{in} > \lambda_{ex}$ ii) and oblates for $\lambda_{in} < \lambda_{ex}$ iii). At high frequencies, the electric charges cannot follow the oscillations of the electric field, hence this relaxes the shape of the 3D FLBs to spherical iv). The green arrow indicates the change of the cylindrical lipid structure caused by the morphology changes of semispherical lipid structures owing to energy minimization in lipid membrane surface. d) The shape change of the 3D FLBs at various frequencies. The dashed line is the calculated value of the capacitor charging and Maxwell-Wagner

frequency (ω_c = 14.15 Hz, ω_{MW} = 2247.95 Hz). The square dots indicate the prolate case, and the circle dots indicate the oblate case at the intermediate frequency. The error bars represent the standard deviations of the shape elongation for each case (n = 10).

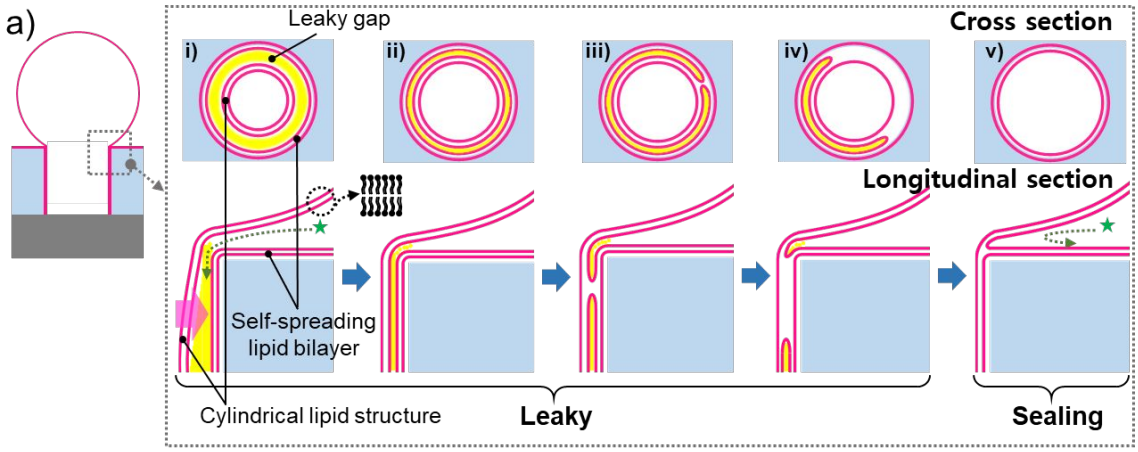

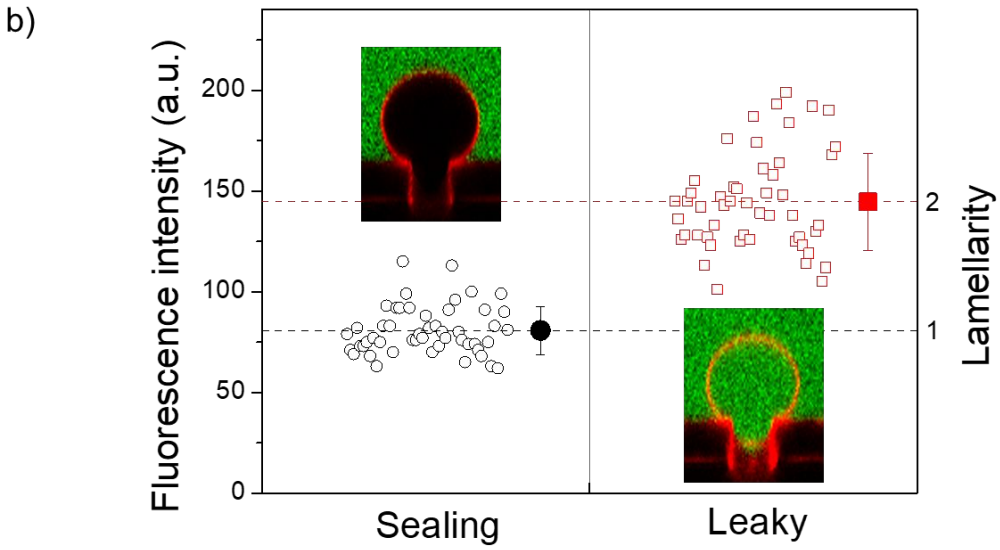

Figure 5. Membrane fusion and sealing for the oblate case and the spherical case. a) Schematic illustrations of shape elongation and membrane fusion between the cylindrical lipid structure and the self-spreading lipid bilayer. i) Expanding of the cylindrical lipid structure, ii) Membrane contact between the cylindrical lipid structure and the self-spreading lipid bilayer, iii) Membrane fusion occurs, iv) Partial fusion, v) Complete fusion. During the fusion process, the 3D FLBs were leaky before the complete fusion due to the leaky gap (yellow area). Only the 3D FLBs that were completely fused accomplished their sealing. b) The fluorescence intensity of the cylindrical lipid structures. The measuring point was inside the microwell. The empty circles and squares indicate 50 each of the sealing and leaky case, respectively. The solid circle and square are the averages of their scattering. The error bar is the standard deviation.

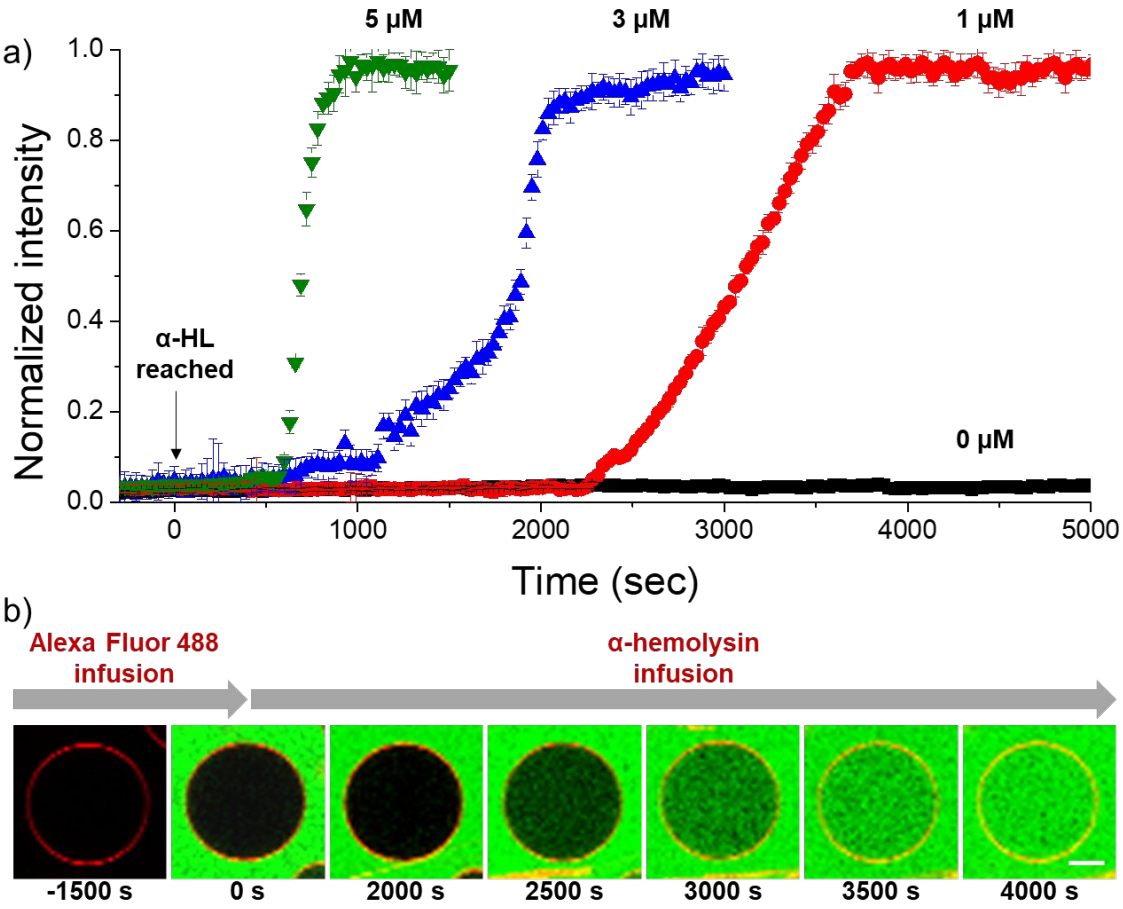

Figure 6. Transport assay using pore-forming membrane protein α-hemolysin. a) The normalized fluorescent intensities in 3D FLBs for 0 (black), 1 (red), 3 (blue), and 5 (green) μM α-hemolysin infusion over time. No normalized intensity change in the 3D FLBs upon the infusion of Alexa Fluor 488 and the increased normalized intensities in the 3D FLBs after the infusion of α-hemolysin indicate the sealing and the biofunctionality of the 3D FLBs, respectively. The error bar represents the standard

deviation (n ≥ 6). b) Time-lapse confocal image of the 3D FLBs upon infusions of 3 μM Alexa Fluor 488 and 1 μM α-hemolysin in sequence. The scale bar is 5 μm.

ASSOCIATED CONTENT

Supporting Information

The Supporting Information is available free of charge

The schematics of lipid selective deposition; Details of the sealing characteristics of the 3D FLBs at 10 and 100 Hz; Sealing to leaky transition of the 3D FLBs formed at 100 Hz; Lamellarity determination based on the quantification of the intensity of the fluorescently-labeled lipids; and The fluorescence intensity of the 3D FLBs at sealing and leaky case (PDF)

AUTHOR INFORMATION

Corresponding Author

*E-mail: tskim@kist.re.kr

Notes

The authors declare no competing financial interest.

ACKNOWLEDGMENT

This research was supported by KIST (Korea Institute of Science and Technology) Institutional Program (2E27910). We are also indebted to Dr. Young Jun Kim and Dr. Kuiwon Choi, Director, Korea Institute of Science and Technology Europe, Germany for the alpha-hemolysin experiments.

REFERENCES

(1) Edidin, M. Lipid Microdomains in Cell Surface Membranes. *Curr. Opin. Struct. Biol.* **1997,** *7* (4), 528-532, DOI: 10.1016/S0959-440X(97)80117-0.

(2) Siontorou, C. G.; Nikoleli, G. P.; Nikolelis, D. P.; Karapetis, S. K. Artificial Lipid Membranes: Past, Present, and Future. *Membranes* **2017,** *7* (3), 38, DOI: 10.3390/membranes7030038.

(3) Mazur, F.; Bally, M.; Stadler, B.; Chandrawati, R. Liposomes and Lipid Bilayers in Biosensors. *Adv. Colloid Interface Sci.* **2017,** *249*, 88-99, DOI: 10.1016/j.cis.2017.05.020.

(4) Osaki, T.; Takeuchi, S. Artificial Cell Membrane Systems for Biosensing Applications. *Anal. Chem.* **2017,** *89* (1), 216-231, DOI: 10.1021/acs.analchem.6b04744.

(5) Hirano-Iwata, A.; Taira, T.; Oshima, A.; Kimura, Y.; Niwano, M. Improved Stability of Free-Standing Lipid Bilayers based on Nanoporous Alumina Films. *Appl. Phys. Lett.* **2010,** *96* (21), 213706, DOI: 10.1063/1.3441298.

(6) Le Pioufle, B.; Suzuki, H.; Tabata, K. V.; Noji, H.; Takeuchi, S. Lipid Bilayer Microarray for Parallel Recording of Transmembrane Ion Currents. *Anal. Chem.* **2008,** *80* (1), 328-332, DOI: 10.1021/ac7016635.

(7) Schmitt, E. K.; Vrouenraets, M.; Steinem, C. Channel Activity of OmpF Monitored in Nano-BLMs. *Biophys. J.* **2006,** *91* (6), 2163-2171, DOI: 10.1529/biophysj.106.083592.

(8) White, R. J.; Ervin, E. N.; Yang, T.; Chen, X.; Daniel, S.; Cremer, P. S.; White, H. S. Single Ion-Channel Recordings using Glass Nanopore Membranes. *J. Am. Chem. Soc.* **2007,** *129* (38), 11766-11775, DOI: 10.1021/ja073174q.

(9) Seddon, A. M.; Curnow, P.; Booth, P. J. Membrane Proteins, Lipids and Detergents: Not Just a Soap Opera. *Biochim. Biophys. Acta* **2004,** *1666* (1-2), 105-17, DOI: 10.1016/j.bbamem.2004.04.011.

(10) Walde, P.; Cosentino, K.; Engel, H.; Stano, P. Giant Vesicles: Preparations and Applications. *ChemBioChem* **2010,** *11* (7), 848-65, DOI: 10.1002/cbic.201000010.

(11) Reeves, J. P.; Dowben, R. M. Formation and Properties of Thin-Walled Phospholipid Vesicles. *J. Cell. Physiol.* **1969,** *73* (1), 49-60, DOI: 10.1002/jcp.1040730108

(12) Tsumoto, K.; Matsuo, H.; Tomita, M.; Yoshimura, T. Efficient Formation of Giant Liposomes through the Gentle Hydration of Phosphatidylcholine Films Doped with Sugar. *Colloids Surf. B. Biointerfaces* **2009,** *68* (1), 98-105, DOI: 10.1016/j.colsurfb.2008.09.023.

(13) Angelova, M. I.; Dimitrov, D. S. Liposome Electroformation. *Fraday Discuss. Chem. Soc.* **1986,** *81*, 303-311, DOI: 10.1039/DC9868100303.

(14) Baumgart, T.; Hess, S. T.; Webb, W. W. Imaging Coexisting Fluid Domains in Biomembrane Models Coupling Curvature and Line Tension. *Nature* **2003,** *425* (6960), 821, DOI: 10.1038/nature02013.

(15) Shimanouchi, T.; Umakoshi, H.; Kuboi, R. Kinetic Study on Giant Vesicle Formation with Electroformation Method. *Langmuir* **2009,** *25* (9), 4835-4840, DOI: 10.1021/la8040488.

(16) Kuribayashi, K.; Tresset, G.; Coquet, P.; Fujita, H.; Takeuchi, S. Electroformation of Giant Liposomes in Microfluidic Channels. *Meas. Sci. Technol.* **2006**, *17* (12), 3121-3126, DOI: 10.1088/0957-0233/17/12/S01

(17) Jørgensen, M.; Bæk, R.; Pedersen, S.; Søndergaard, E. K.; Kristensen, S. R.; Varming, K. Extracellular Vesicle (EV) Array: Microarray Capturing of Exosomes and other Extracellular Vesicles for Multiplexed Phenotyping. *J. Extracell. Vesicles* **2013,** *2* (1), 20920, DOI: 10.3402/jev.v2i0.20920.

(18) Jung, H.-S.; Ahn, N.; Lee, J.; Seo, S.; Suh, K.-Y.; Kim, J.; Kim, K. Biomimetic Detection of Aminoglycosidic Antibiotics using Polydiacetylene–Phospholipids Supramolecules. *Chem. Commun.* **2012,** *48* (43), 5313-5315, DOI: 10.1039/C2CC31466E.

(19) Städler, B.; Bally, M.; Grieshaber, D.; Vörös, J.; Brisson, A.; Grandin, H. M. Creation of a Functional Heterogeneous Vesicle Array via DNA Controlled Surface Sorting onto a Spotted Microarray. *Biointerphases* **2006,** *1* (4), 142-145, DOI: 10.1116/1.2434178.

(20) Stamou, D.; Duschl, C.; Delamarche, E.; Vogel, H. Self-assembled Microarrays of Attoliter Molecular Vessels. *Angew. Chem.* **2003,** *115* (45), 5738-5741, DOI: 10.1002/anie.200351866.

(21) Kang, Y. J.; Wostein, H. S.; Majd, S. A Simple and Versatile Method for the Formation of Arrays of Giant Vesicles with Controlled Size and Composition. *Adv. Mater.* **2013,** *25* (47), 6834-8, DOI: 10.1002/adma.201303290.

(22) Osaki, T.; Kamiya, K.; Kawano, R.; Takeuchi, S. In *Uniform Size Liposomes on a Chip: Observation of Transport Kinetics through Nanopore Membrane Protein*, 16th International Conference on Miniaturized Systems for Chemistry and Life Sciences, Okinawa, Japan, October 28 - November 1; Royal Society of Chemistry: Okinawa, Japan, 2012; pp 94-96.

(23) Han, W. B.; Kwak, R.; Kim, T. S. In *Generation of 3-Dimensional Lipid Structure Array Attached to Si Microwells*, 21th International Conference on Miniaturized Systems for Chemistry and Life Sciences, Savannah USA, 22-26 October; Savannah USA, 2017.

(24) Diguet, A.; Le Berre, M.; Chen, Y.; Baigl, D. Preparation of Phospholipid Multilayer Patterns of Controlled Size and Thickness by Capillary Assembly on a Microstructured Substrate. *Small* **2009,** *5* (14), 1661-6, DOI: 10.1002/smll.200900368.

(25) Jackman, R. J.; Duffy, D. C.; Ostuni, E.; Willmore, N. D.; Whitesides, G. M. Fabricating Large Arrays of Microwells with Arbitrary Dimensions and Filling Them using Discontinuous Dewetting. *Anal. Chem.* **1998,** *70* (11), 2280-2287, DOI: 10.1021/ac971295a.

(26) Politano, T. J.; Froude, V. E.; Jing, B.; Zhu, Y. AC-electric Field Dependent Electroformation of Giant Lipid Vesicles. *Colloids Surf. B. Biointerfaces* **2010,** *79* (1), 75-82, DOI: 10.1016/j.colsurfb.2010.03.032.

(27) Li, W.; Wang, Q.; Yang, Z.; Wang, W.; Cao, Y.; Hu, N.; Luo, H.; Liao, Y.; Yang, J. Impacts of Electrical Parameters on the Electroformation of Giant Vesicles on ITO Glass Chips. *Colloids Surf. B. Biointerfaces* **2016,** *140*, 560-6, DOI: 10.1016/j.colsurfb.2015.11.020.

(28) Aranda, S.; Riske, K. A.; Lipowsky, R.; Dimova, R. Morphological Transitions of Vesicles Induced by Alternating Electric Fields. *Biophys. J.* **2008,** *95* (2), L19-21, DOI: 10.1529/biophysj.108.132548.

(29) Nganguia, H.; Young, Y. N. Equilibrium Electrodeformation of a Spheroidal Vesicle in an AC Electric Field. *Phys. Rev. E: Stat. Phys., Plasmas, Fluids,* **2013,** *88* (5), 052718, DOI: 10.1103/PhysRevE.88.052718.

(30) Dimova, R.; Riske, K. A.; Aranda, S.; Bezlyepkina, N.; Knorr, R. L.; Lipowsky, R. Giant Vesicles in Electric Fields. *Soft Matter* **2007,** *3* (7), 817-827, DOI: 10.1039/B703580B.

(31) Malmberg, C. G.; Maryott, A. A. Dielectric Constants of Aqueous Solutions of Dextrose and Sucrose. *J. Res. Natl. Bur. Stand. Sec. A* **1950,** *45* (4), 299-303.

(32) Feng, F.; Klug, W. S. Finite Element Modeling of Lipid Bilayer Membranes. *J. Comput. Phys.* **2006,** *220* (1), 394-408, DOI: 10.1016/j.jcp.2006.05.023.

(33) Perera, L.; Essmann, U.; Berkowitz, M. L. Role of Water in the Hydration Force Acting between Lipid Bilayers. *Langmuir* **1996,** *12* (11), 2625-2629, DOI: 10.1021/la9515534.

(34) Chernomordik, L. V.; Kozlov, M. M. Mechanics of Membrane Fusion. *Nat. Struct. Mol. Biol.* **2008,** *15* (7), 675-83, DOI: 10.1038/nsmb.1455.

(35) Akashi, K.-i.; Miyata, H.; Itoh, H.; Kinosita Jr, K. Preparation of Giant Liposomes in Physiological Conditions and their Characterization under an Optical Microscope. *Biophys. J.* **1996,** *71* (6), 3242-3250, DOI: 10.1016/S0006-3495(96)79517-6.

(36) Song, L.; Hobaugh, M. R.; Shustak, C.; Cheley, S.; Bayley, H.; Gouaux, J. E. Structure of Staphylococcal α-hemolysin, a Heptameric Transmembrane Pore. *Science* **1996,** *274* (5294), 1859-1865, DOI: 10.1126/science.274.5294.1859.

(37) Watanabe, R.; Soga, N.; Hara, M.; Noji, H. Arrayed Water-in-oil Droplet Bilayers for Membrane Transport Analysis. *Lab Chip* **2016,** *16* (16), 3043-8, DOI: 10.1039/c6lc00155f.

Table of Contents (TOC)

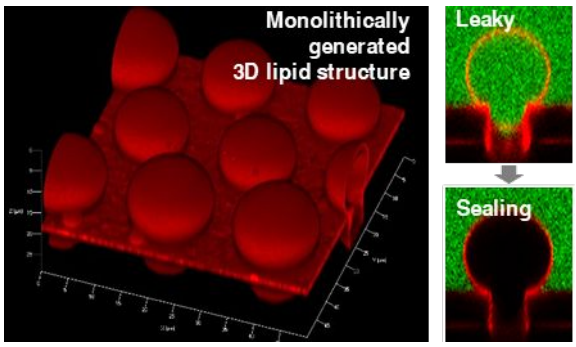
Monolithically
generated
3D lipid structure
Leaky
Sealing

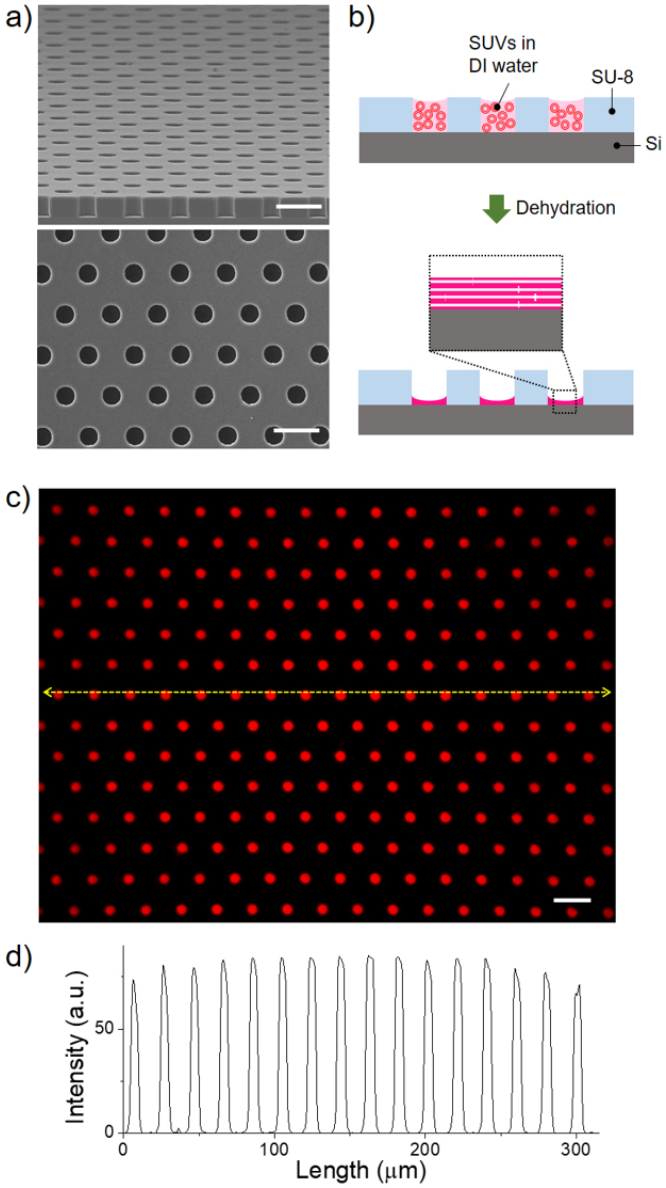

Figure 1. Selective deposition of the lipid multilayer only inside microwells. a) SEM images of fabricated SU-8 microwell arrays on a silicon substrate. The diameter and the depth of the microwell were 8 μm, and the pitch of each microwell was 20 μm. b) Schematics of selective deposition on the microwells. After filling the SUVs only inside of microwells, the chip was placed in the freeze dryer for dehydration. After the dehydration, the stacked lipid film was deposited selectively only inside of microwells. c) Fluorescence microscopy image of selectively deposited lipid after the dehydration. d) Fluorescence intensity profile along the dotted line in c). All scale bars are 20 μm.

113x190mm (150 x 150 DPI)

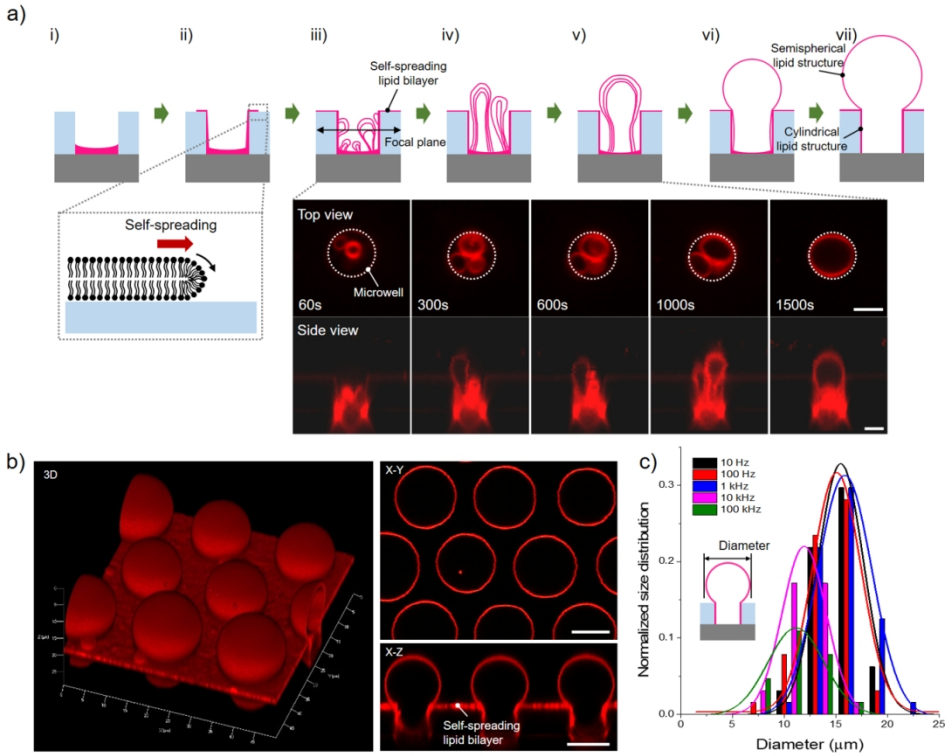

Figure 2. The generation of 3D FLBs by rehydration and electroformation. a) Schematics of the generation of 3D FLBs: i) The deposited lipid multilayer. ii) At the beginning of rehydration and electroformation by 10 mM sucrose solution, the stacked lipid film was self-spread initially. iii) After the self-spreading of the lipid bilayer (covering the entire surface of the SU-8), the lipid film was swelling and several MLVs were generated that were tethered to the substrate. iv) The MLVs were grown and fused by several multilayer structures. v) As time passed, the growing multilayer structures got closer to each other due to the confined space of the microwell, and they fused to become one multilayer structure. vi) Then, the multilayer structure underwent gradual fusion and formed a unilamellar structure. vii) Finally, the 3D FLBs were formed on the microwell. The lower images were obtained by confocal microscopy at 1kHz. The focal plane was inside the microwell, hence we were able to monitor each sequence of the generation and fusion of the 3D FLBs. The scale bar is 5 μm. b) The confocal microscopy images of generated 3D FLBs as 1kHz electroformation frequency. The 3D image was reconstructed from scanned confocal microscopy images. Thin and identical fluorescence intensities of the structures in X-Z imply that each of the 3D FLBs consisted of a single bilayer. The scale bar is 10 μm. c) The size distributions of the 3D FLBs at various frequencies (10 Hz – 100 kHz). Each dataset was fitted with the Gaussian distribution function.

243x190mm (150 x 150 DPI)

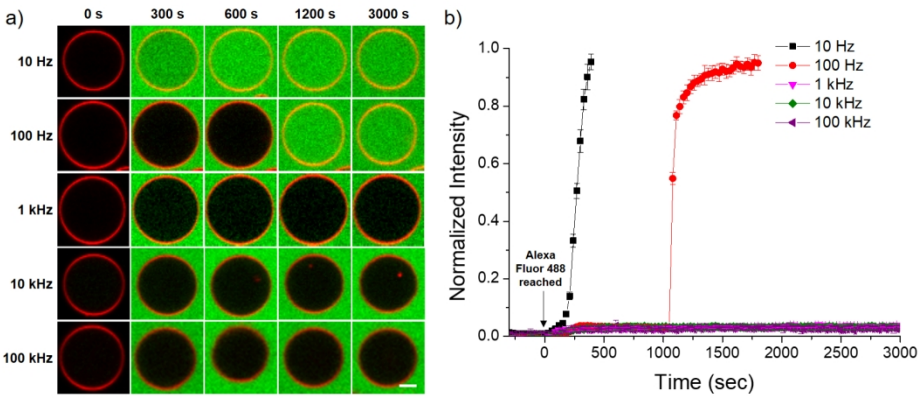

Figure 3. The sealing characteristics of the 3D FLBs at various frequencies. a) Images of the 3D FLBs observed by confocal microscopy over time at various electroformation frequencies. At 0 s, the Alexa Fluor 488 was reached. The scale bar is 5 μm. b) The normalized intensity of the inner 3D FLBs after the Alexa Fluor 488 was reached. The error bar represents the standard deviation (n ≥ 4). At 10 and 100 Hz, external fluorescent dye molecules entered inside the 3D FLBs and increased the normalized intensities because of their leaky structures. Above 1 kHz, the sealing was maintained.

312x127mm (150 x 150 DPI)

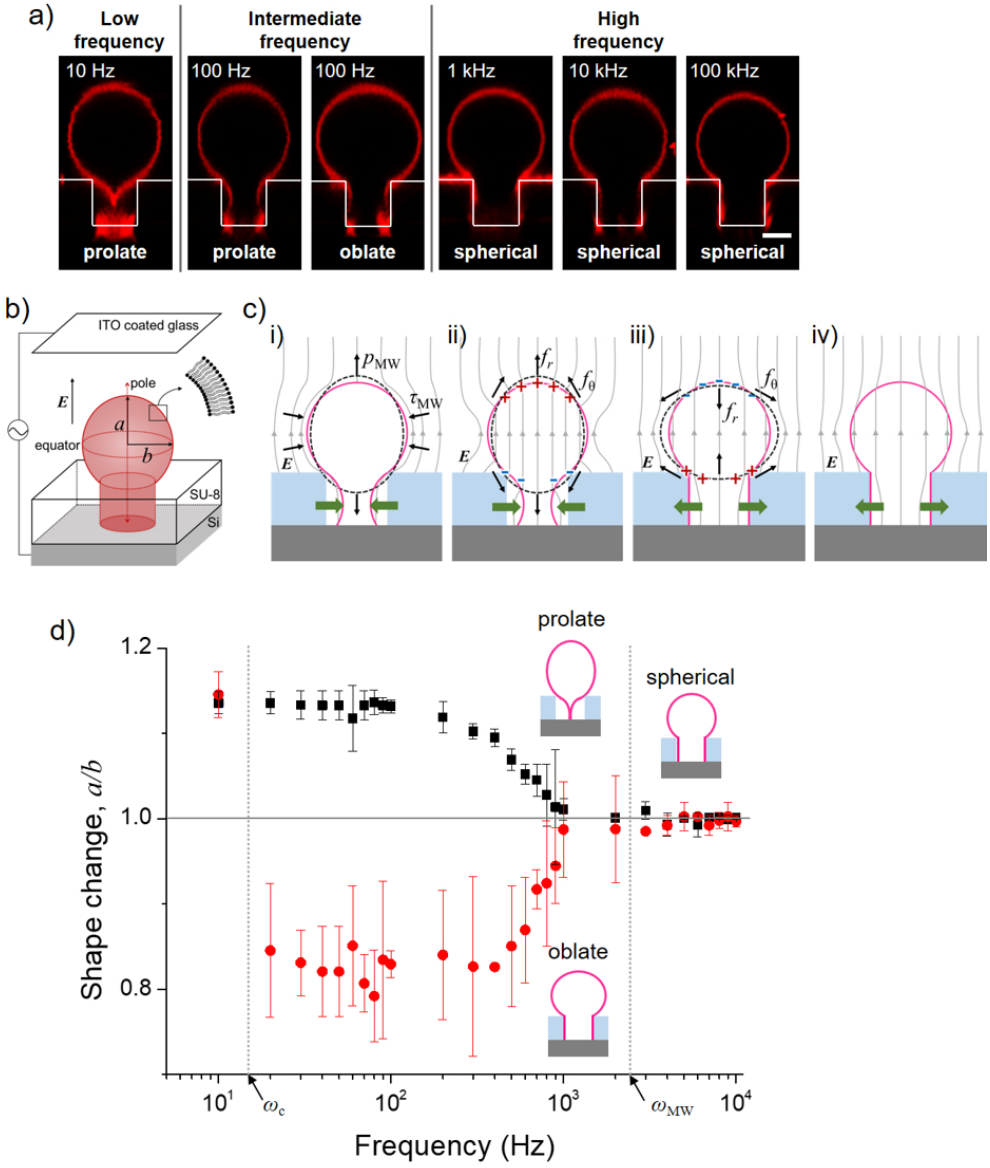

Figure 4. The shape of 3D FLBs at the various electroformation frequencies. a) Side view of the generated 3D FLBs observed by confocal microscopy as frequencies. The side view images were reconstructed from the scanned confocal microscopy images. Tethered and thin cylindrical lipid structures were observed at 10 Hz and at the prolate case of 100 Hz, respectively. At the oblate case of 100 Hz and the spherical case of 1 to 100 kHz, the cylindrical lipid structure was expanded and contacted the self-spreading lipid bilayer. The scale bar is 5 μm. b) The geometry of the 3D FLB, and c) the net charge distribution at the 3D FLB interfaces. At low frequencies, the 3D FLBs were squeezed by the radial Maxwell stress or pressure arising from the tangential electric field, hence the 3D FLBs adopt a prolate shape i). At intermediate frequencies, due to the difference in the conductivity conditions, the net charges across the membrane, illustrated with pluses and minuses, differed depending on the values of the conductivity inside and outside of the membrane. The forces applied to the charges by the normal and the tangential electric fields deformed the 3D FLBs into prolates for λin > λex ii) and oblates for λin < λex iii). At high frequencies, the electric charges cannot follow the oscillations of the electric field, hence this relaxes the shape of the 3D FLBs to spherical iv). The green arrow indicates the change of the cylindrical lipid structure caused by the morphology

changes of semispherical lipid structures owing to energy minimization in lipid membrane surface. d) The shape change of the 3D FLBs at various frequencies. The dashed line is the calculated value of the capacitor charging and Maxwell-Wagner frequency (ωc = 14.15 Hz, ωMW = 2247.95 Hz). The square dots indicate the prolate case, and the circle dots indicate the oblate case at the intermediate frequency. The error bars represent the standard deviations of the shape elongation for each case (n = 10).

160x190mm (150 x 150 DPI)

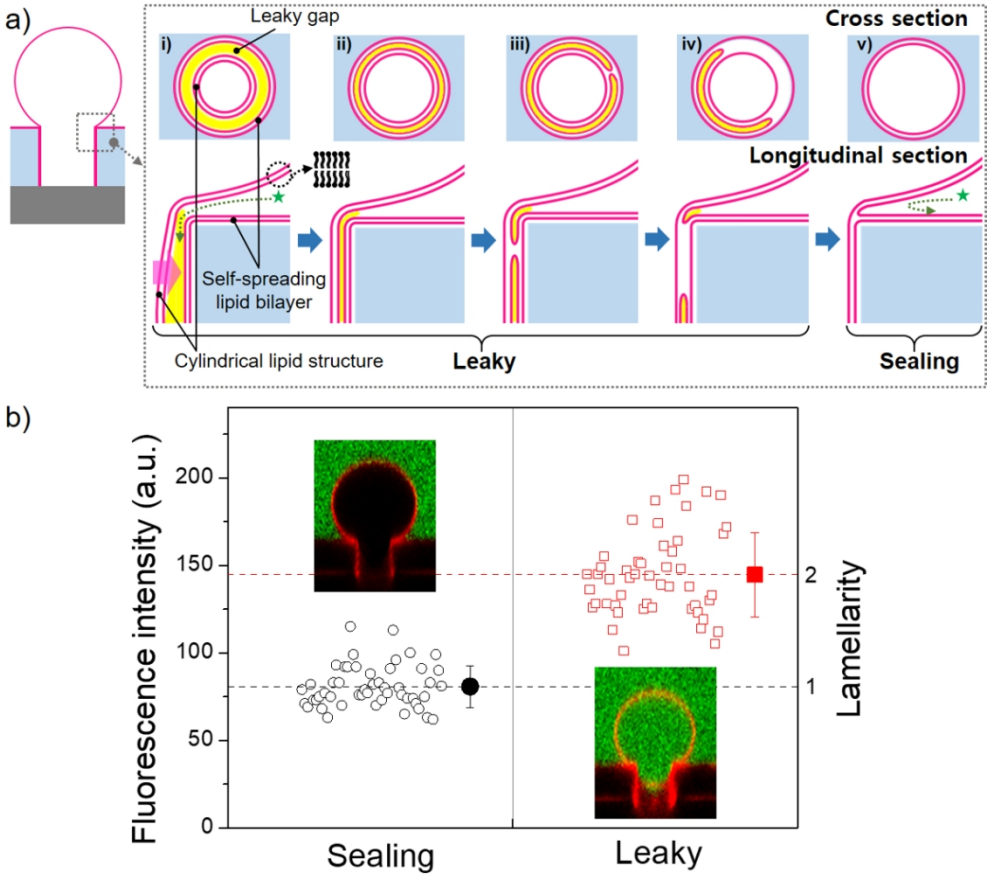

Figure 5. Membrane fusion and sealing for the oblate case and the spherical case. a) Schematic illustrations of shape elongation and membrane fusion between the cylindrical lipid structure and the self-spreading lipid bilayer. i) Expanding of the cylindrical lipid structure, ii) Membrane contact between the cylindrical lipid structure and the self-spreading lipid bilayer, iii) Membrane fusion occurs, iv) Partial fusion, v) Complete fusion. During the fusion process, the 3D FLBs were leaky before the complete fusion due to the leaky gap (yellow area). Only the 3D FLBs that were completely fused accomplished their sealing. b) The fluorescence intensity of the cylindrical lipid structures. The measuring point was inside the microwell. The empty circles and squares indicate 50 each of the sealing and leaky case, respectively. The solid circle and square are the averages of their scattering. The error bar is the standard deviation.

203x190mm (150 x 150 DPI)

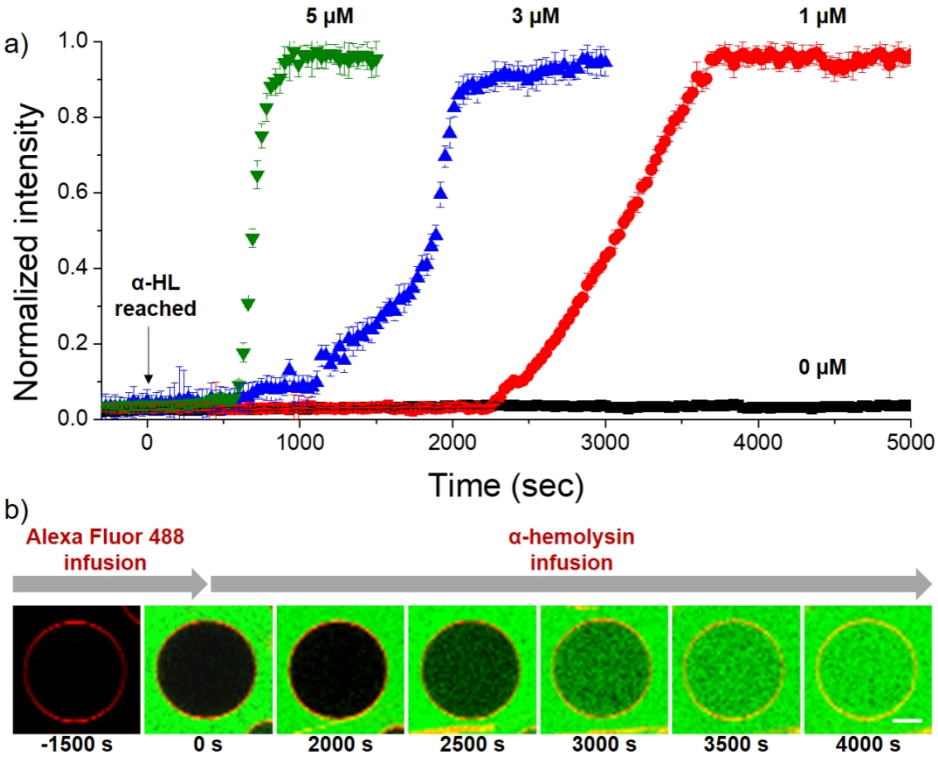

Figure 6. Transport assay using pore-forming membrane protein α-hemolysin. a) The normalized fluorescent intensities in 3D FLBs for 0 (black), 1 (red), 3 (blue), and 5 (green) μM α-hemolysin infusion over time. No normalized intensity change in the 3D FLBs upon the infusion of Alexa Fluor 488 and the increased normalized intensities in the 3D FLBs after the infusion of α-hemolysin indicate the sealing and the biofunctionality of the 3D FLBs, respectively. The error bar represents the standard deviation (n ≥ 6). b) Time-lapse confocal image of the 3D FLBs upon infusions of 3 μM Alexa Fluor 488 and 1 μM α-hemolysin in sequence. The scale bar is 5 μm.

228x180mm (150 x 150 DPI)